Twelfth Australasian Fluid Mechanics Conference
The University of Sydney, Australia 1995

SOME ASPECTS OF THREE-DIMENSIONAL TURBULENT SEPARATION

Roger L. Simpson

Aerospace and Ocean Engineering Department
Virginia Polytechnic Institute and State University
Blacksburg, Virginia
The United States of America

ABSTRACT

The nature of the unsteady multi-modal vortical flow separation around the nose of a hull/appendage or wing/body junction is discussed.

THREE-DIMENSIONAL SEPARATIONS

Separation is the entire process of *departure* or *breakaway*, or the breakdown of boundary-layer flow. An abrupt thickening of the rotational-flow region next to a wall and significant values of the normal-to-wall velocity component V must accompany breakaway, or otherwise this region will not have any significant interaction with the inviscid free-stream flow (Simpson, 1989). Along a three-dimensional separation line on the surface of a body rises a stream surface, across which no flow from one side of the separation line can pass to the other side. Surface skin friction lines converge on each side of the separation line, as well as converge toward one another.

Among others, Tobak and Peake (1982) and Yates and Chapman (1992) discuss the topology and kinematics of 3-D separated flows. Yates and Chapman point out that "global" separations (sometimes called "closed" separations) always have a saddle point of separation on the surface, such as the horseshoe type.

The nature of one type of 3-D separation, as revealed by recent experiments, is discussed briefly here. Other 3-D separations are discussed in more detail by Simpson (1995). So-called "closed" vortical turbulent separations, such as shown in Figure 1, have an exchange of mass particles, with relatively high turbulence intensities in regions of local backflow. The recently researched wing/body junction flow has revealed a chaotic-like multi-modal vortex structure at and near the nose. This is responsible for high surface pressure fluctuations and heat transfer in this region.

SOME UNSTEADY FEATURES OF TURBULENT WING-BODY JUNCTION SEPARATIONS

A large number of investigations have presented time-averaged surface oil flows around an obstacle/body intersection. Here we will not review all of these earlier studies; Tobak and Peake (1982), Baker (1980), Dargahi (1989), Pierce and Shin (1992), and Ölçmen and Simpson (1992) give references to much earlier work. Figure 1 shows a 3-D separation in front of the nose of the 3:2 elliptic nose/NACA 0020 tail wing (or "Rood" wing after its designer E.P. Rood) that has been used in much of the author's related wind tunnel work. A "horseshoe vortex" forms at the nose of the wing at a junction because the spanwise vorticity in the approach boundary layer rolls up and is stretched around the body. A 3-D stagnation point (singularity) is shown in the time-averaged oil flow; a "closed" time-averaged separation line starts from this point and is located around each side of the wing. Time-averaged backflow is present between this stagnation point and the nose. A line of low shear also is located between this closed separation and the wing nose and merges with the closed separation at the side of the model.

In the past, a steady multiple vortex conceptual model was used to describe the flow in front of the nose. A common model, such as shown in the laminar smoke flow visualization in the frontispiece photo of Thwaites (1960), shows one vortex shed from the 3-D separation and a second downstream next to the wing nose, each with the rotational sense of the upstream vorticity. Smaller third and fourth vortices next to the surface and between the first and second vortex and the second vortex and the wing nose are of the opposite rotational sense. As discussed below, in reality the nose region vortex system is highly unsteady. It is interesting to note that unsteady horseshoe vortices have been observed in laminar flows (Thomas, 1987; Cantwell, 1990); the horseshoe vortex nearest the nose is split and shed periodically, with a new vortex moving forward to take its place.

Here the work by the author and colleagues will be emphasized since the unsteady "bimodal" nature of the horseshoe vortex "system" has been the subject of much recent research and some of the results have not yet been reported. Using 3-velocity-component LDV measurements around the Rood wing at an approach momentum thickness Reynolds number Re_θ of 6300, Devenport and Simpson (1987) were the first to report the bimodal velocity probability phenomenon, which is responsible for high surface pressure fluctuation levels and high heat transfer rates in the region. This work showed the elliptical shape of the time-averaged vortex. Further research (Devenport and

Simpson, 1988, 1990) showed that the flow in this zone switched aperiodically from one mode to another; probably in a Markovian PDF. Martinuzzi *et al.* (1992) showed that the time between bimodal switches T appears to be a Markovian process, i.e., one whose PDF is (1/B)exp(-T/B), where B is a normalizing parameter. Turbulence energy production and turbulent stresses an order of magnitude higher than in the upstream boundary layer were found in this zone because of this low frequency self-induced chaotic switching. Normal Reynolds stress turbulence kinetic energy production terms $-\overline{u^2}\partial U/\partial X$ and $-\overline{v^2}\partial V/\partial Y$ are as equally important as the usual shear stress production $-\overline{uv}\partial U/\partial Y$ (Devenport and Simpson, 1987).

Flow visualization has provided some understanding of the vortex systems that produce the bimodal velocities. Dargahi (1989) showed the consequences of an unsteady vortex pattern. An unsteady vortex formation with 5 vortices in front of a circular cylinder was shed quasi-periodically. Flow visualization results indicated that the mean flow direction in the separated flow region close to the wall was mainly in the reversed direction. However, there was no quantitative data to complement these visualizations.

Hydrogen-bubble flow visualization experiments have been done on a 2 foot chord clear plexiglas model of the Rood wing in a water tunnel (Kim *et al.*, 1991) at approach momentum Reynolds numbers Re_θ of 330 and 1100. Single-velocity component LDV measurements were also made. Figure 2 shows a schematic of the self-induced unsteady phenomena revealed from videos. At the beginning of the sequence of flow events (a), a large horseshoe vortex exists in front of the nose, produced by high velocity free-stream fluid impinging on and moving down the nose. Because the vortex lines of this flow are stretched around the wing, the cross-sectional area of the vortex decreases at increasing times in (b - g). Meanwhile, a secondary separation vortex forms downstream of separation in (b), increasing with circulation strength at increasing times in (c) and (d). Other tertiary vortices can be formed as in (c) and (d). At some time, the secondary and tertiary vortices either merge together, merge with the front of the horseshoe vortex or move up over the horseshoe vortex in "leap frog" fashion before merging with the horseshoe vortex. The resulting merger creates a stronger large horseshoe vortex which is stretched around the wing. During this phase of this aperiodic sequence, forward flow moves much closer to the wing (e) and the this acceleration briefly stabilizes the flow. The flow then becomes unstable in (f), a new large-scale horseshoe vortex forms and the aperiodic process begins anew in (g).

In reanalysis of some of these video sequences, Devenport (unpublished) pointed out that: (i) there appears to be space enough for only one horseshoe vortex at any instant; (ii) secondary and tertiary vortices frequently are swept around the wing before merging with the horseshoe vortex; and (iii) the horseshoe vortex appears to be dissipated by viscosity or just become incoherent during phase (e).

The approach flow Reynolds number is not a controlling factor for the existence of the bimodal behavior. The wing shape is the major factor because it largely determines the pressure gradients in front of and around the wing and the rate of stretching of the 'horseshoe vortex" around the wing. While the "horseshoe vortex" nearest the wing nose is being stretched, newer younger vortices are formed downstream of the 3-D separation. The younger vortices grow with time while the oldest vortex is reduced in size by stretching. Eventually one or more of these new vortices merges with what is left of the oldest one to form another "old" vortex nearest the nose. The process is then repeated, although the process is never periodic and appears to be Markovian.

Rife, Devenport, and Simpson (1991) examined the relationship between the bimodal velocity and surface pressure fluctuations in front of the nose of this wing/body junction. Velocity autospectra showed the bimodal region to be dominated by low frequency fluctuations around fT/U_{ref} = 1/20, where f is the average frequency and T is the maximum wing thickness. Strong statistical coherency was found between velocity and surface pressure fluctuations at these frequencies where large-scale unsteady bimodal structures were observed.

Shinpaugh (1994) rapidly scanned (50Hz) normal to the body surface a two-velocity-component LDV in the bimodal zone of the Rood wing/body junction wind tunnel flow of Devenport and Simpson. Using the bimodal surface pressure level under the bimodal region (X/T = -0.26) as an event trigger, the resulting event-threshold velocity-conditional-averages support a flow model of a single primary junction vortex that changes size and location in front of the wing. When the surface pressure is higher than the mean, the junction vortex is concentrated near the nose. When the pressure signal is below the mean, the vortex lies farther from the nose and the backflow near the nose is lower. These results do not conflict with the water tunnel results of Kim *et al.* Since the passage of upstream separation vortices over or merger with the primary vortex is not synchronized with the primary horseshoe vortex, ensemble-averaged velocities triggered off of the wall pressure level will average out these smaller-scaled vortex velocities.

A "bluntness factor" correlation on the effect of wing shape on the horseshoe vortex stretching rate was developed by Fleming *et al.* (1991). The "bluntness factor" is defined as

$$BF = \frac{1}{2}\frac{R_o}{X_{TMAX}}\left[\frac{T_{MAX}}{S_{TMAX}} + \left(\frac{S}{X}\right)_{TMAX}\right]$$

where R_o is the leading edge radius, X_{Tmax} is the chordwise position of the maximum thickness T_{max}, and S_{Tmax} is the distance from the leading edge along the airfoil surface to the maximum thickness. Assuming an inviscid potential flow 2-D model, he calculated the average stretching rate from the nose to the maximum thickness for 28 airfoil shapes at zero angle of attack and 14 shapes at 12° angle of attack for 10^{-3} < BF < 1.07, including the ones discussed below. The average vortex stretching rate from the nose to the maximum thickness is

$$VS = \frac{R_o}{U_\infty}\left(\frac{V_s}{S}\right)_{TMAX}$$

and is fit with high correlation coefficients by

$$VS = 10^b (BF)^m$$

with m = 0.8816 and b = 0.0482 for zero angle of attack

cases and m = 0.8075 and b = 0.0142 for the 12° angle of attack cases.

Ölçmen and Simpson (1992) made experimental surface pressure fluctuation and other measurements on the effect of nose shape (bluntness) on the bimodal vortical flow behavior at the nose of wing/body junctions for 6 different shaped wings. Greater nose bluntness BF produces a stronger nose vortex system. The Sandia 1850 with a BF = 0.0133 and a NACA 0012 with a BF = 0.0287 produced no apparent bimodal vortical structure and lower pressure fluctuations, while a NACA 0015 with a BF = 0.0452 and models with higher BF values did. A circular-nosed tear-drop model with BF = 1.07 produced the largest vortex stretching parameter of 1.13.

Lewis *et al.* (1993) measured the time- and spatially-resolved surface heat flux in the nose region of 3 different wing/body junctions that had bimodal velocity and pressure phenomena: NACA 0015, Rood wing (BF = 0.32), and the circular-nosed tear-drop model. No bimodal heat-flux fluctuation histograms were observed. Some major findings from this study were: 1) the enhancement in heat flux in the region downstream of the time-mean separation line and upstream of the time-mean vortex center is due to the high levels of turbulent stress near the wall produced by the large-scale unsteadiness of the horseshoe vortex, and 2) the maximum level of heat flux occurs in the immediate vicinity of the wing/endwall junction due to the effects of the vortex on the mean flow-field. The main vortex transports cold outer boundary layer fluid down the leading edge of the wing, perpendicular to the endwall, where it impinges on the endwall. The strength of this impinging jet is related to the size and location of the primary vortex which is controlled by the bluntness of the wing nose.

This is a vorticity-dominated flowfield that is controlled by the stretching of the horseshoe vortex and the separation vortex. This bimodal aperiodic phenomenon accompanies all wing/body junction flows with sufficient "bluntness" and is responsible for observed high turbulence intensities, high pressure fluctuations, and high heat transfer rates. This is of great importance to gas turbine heat transfer, where hub and casing boundary layers produce large heat transfer rates at the junctions with blades.

The 3-velocity-component LDV wind tunnel data of Devenport and Simpson (1990b, 1992) and the recent data of Ölçmen and Simpson (1995b) show that the bimodal structure exists for the velocity components **perpendicular** to the horseshoe vortex core around the front of the Rood wing where the flow is accelerating and the elliptically-shaped vortex is being stretched. High speed free-stream fluid is entrained by this vortex; low turbulent kinetic energy is carried by this fluid. Lower velocity fluid is under this high speed flow and is also on the other side of the vortex. Higher turbulent kinetic energy is transported by this fluid. Accompanying the bimodal structure, very high turbulent kinetic energy fluid is located within and beneath the vortex.

An opposite sense corner vortex near the wing is detected. Another opposite sense vortex with large normal to the surface velocities is near the location of the surface oil-flow skin-friction line that passes through the closed separation stagnation point in Figure 1. No other vortex structure with a large normal-to-the-wall velocity component is located between the wing and the closed separation vortex. Thus, the line of low surface shearing stress that begins in front of the nose of the wing must not qualify for a separation line at this plane. Downstream of the maximum thickness, no bimodal structure was observed, the vortex becomes more circular (Fleming *et al.*, 1991), and the coherent nose-region vortex structure may "burst" due to the adverse pressure gradient.

Fleming *et al.* (1991) examined available data sets for Rood wing/body junction flows from several different research groups over a range of approach momentum Reynolds numbers Re_θ and boundary layer to wing thickness ratios δ/T. The product of Re_T and Re_θ, or Fleming's approach flow "momentum deficit factor" MDF, correlated observed effects on the flow in the downstream adverse pressure gradient region around the wing and in the wake. As MDF increases, streamwise velocity distortions decrease, secondary flow patterns are more elliptic, the vortex core and the vorticity are closer to the wall, the spanwise spacing of the legs of the vortices increase in the wake, and the core vorticity and helicity levels increase when non-dimensionalized on δ and U_{ref}.

REFERENCES

Baker, C.J., 1980, "The Turbulent Horseshoe Vortex," *J. Wind Eng. and Indust. Aero.*, 6, pp. 9 - 23.

Cantwell, B., 1990, Stanford Univ., private comm.

Dargahi, B., 1989, "The Turbulent Flow Field Around a Circular Cylinder," *Exp. Fluids*, 8, pp. 1 - 12.

Devenport, W.J. and Simpson, R.L., 1987, "Turbulence Structure Near the Nose of a Wing-Body Junction", AIAA Paper 87-1310.

Devenport, W.J. and Simpson, R.L., 1988, "Time-Dependent Structure in Wing-Body Junction Flows", *Turb. Shear Flows 6*, pp. 232-248, Springer-Verlag, 1988.

Devenport, W.J. and Simpson, R.L., 1990a, "Time-Dependent and Time-Averaged Turbulence Structure Near the Nose of a Wing-Body Junction", *J. Fluid Mech.*, 210, pp. 23-55.

Devenport, W.J. and Simpson, R.L., 1990b, "An Experimental Investigation of the Flow Past an Idealized Wing-Body Junction," VPI&SU Report Aero-165.

Devenport, W.J. and Simpson, R.L., 1992, "The Flow Past a Wing-Body Junction - An Experimental Evaluation of Turbulence Models," *AIAA Journal*, 30, pp. 873-881.

Fleming, J., Simpson, R.L., and Devenport, W.J., 1991, "An Experimental Study of a Turbulent Wing-Body Junction and Wake Flow," Report VPI-AOE-179, VPI&SU; also AIAA-92-0434; *Exp. Fluids*, 14, pp. 366-378, 1993.

Kim, S.A., Walker, D.A., and Simpson, R.L., 1991, "Observation and Measurements of Flow Structures in the Stagnation Region of a Wing-Body Junction," VPI-E-91-20.

Lewis, D.J., Simpson, R.L., and Diller, T., 1993, "Time-Resolved Surface Heat Flux Measurements in the Wing/Body Junction Vortex," AIAA-93-0291; *AIAA J. Thermo. & Heat Trans.*, Vol. 8, pp. 656 - 663, 1994.

Martinuzzi, R. and Tropea, C., 1993, "The Flow Around Surface-Mounted, Prismatic Obstacles Placed in a Fully Developed Channel Flow," *ASME J. Fluids Eng.*, 115, pp. 85 - 92.

Martinuzzi, R., Melling, A., and Tropea, C., 1992, "Der Wangebundene Würfel im Flachkanal: Zeitaufgelöste Betrachtung der Nachlaufströmung," AG STAB Symp., 10 - 12 Nov.; H.-J. Heineman, ed., DLR, 10 Bunsenstrasse,

Göttingen, Germany.

Martinuzzi, R., Melling, A., and Tropea, C., 1993, "Reynolds Stress Field for the Turbulent Flow Around a Surface-Mounted Cube Placed in a Channel," paper 13 - 4, *9th Symp. Turb. Shear Flows*, Kyoto, Japan, August 16 - 18.

Ölçmen, S.M. and Simpson, R.L., 1992, "Influence of Wing Shapes on the Surface Pressure Fluctuations of a Wing-Body Junction," AIAA-92-0433, *AIAA 30th Aero. Sci.*; *AIAA Journal*, Vol. 32, no. 1, pp. 6 - 15, 1994.

Ölçmen, S.M. and Simpson, R.L., 1995a, "An Experimental Study of Three-Dimensional Pressure-Driven Turbulent Boundary Layer," *J.Fluid Mech.*, 290, pp. 225 - 262.

Ölçmen, S.M. and Simpson, R.L., 1995b, "Some Structural Features of a Turbulent Wing/Body Junction Vortical Flow," manuscript in preparation for *J.Fluid Mech.*

Pierce, F. J, and Shin, J., 1992, "The Development of a Turbulent Vortex System," *TASME J. of Fluids Eng.*, 114, pp. 559 - 565.

Rife, M.C., Devenport, W.J., Simpson, R.L., 1992, "An Experimental Study of the Relationship Between Velocity and Pressure Fluctuations in a Wing-Body Junction," VPI-AOE-188, Aerospace and Ocean Engineering Dept.

Shinpaugh, K.A., 1994, "Measurements in the Bimodal region of a Wing-Body Junction Flow with a Rapidly-Scanning Two-Velocity-Component Laser-Doppler Anemometer," Ph.D. Diss., Aerospace and Ocean Eng., VPI&SU; *Meas. Sci. Technol.*, 6, pp. 702 - 716, 1995.

Simpson, R.L., 1989, "Turbulent Boundary Separation," *Ann. Rev. Fluid Mech.*, Vol. 21, pp.205 - 234.

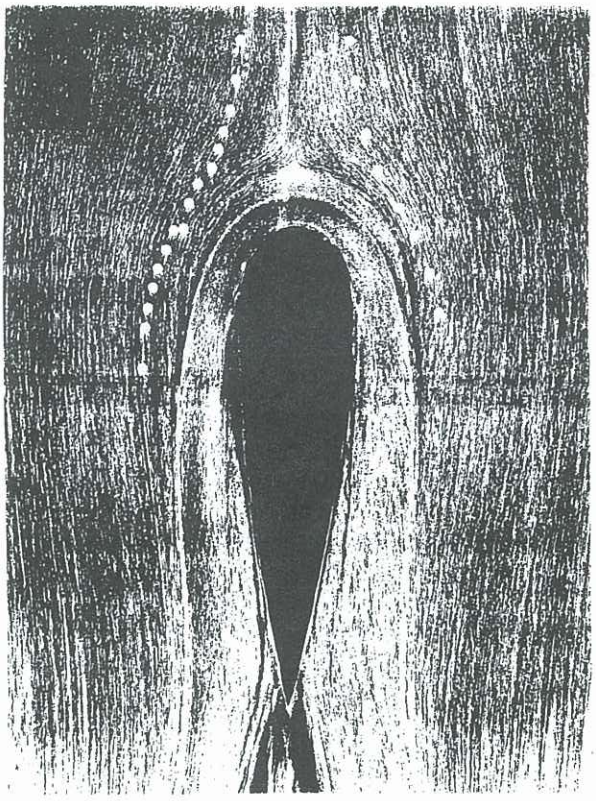

Figure 1. Surface oil-flow visualization of the 3-D flow around the 3:2 elliptic nose/NACA 0020 tail wing mounted perpendicular to the surface. White dots denote the measurement locations. From Ölçmen and Simpson (1995a).

Simpson, R.L., 1995, "Aspects of Turbulent Boundary-Layer Separation," in press, *Prog. Aerosp. Sci.*

Thomas, A.S.W., 1987, "The Unsteady Characteristics of Laminar Juncture Vortices," *Phys. Fluids*, 20, pp. 283 - 285.

Thwaites, B., 1960, *Incompressible Aerodynamics*, Oxford Univ. Press; reprinted, Dover, 1987.

Tobak, M. and Peake, D., 1982, "Topology of Three-Dimensional Separated Flows," *Ann. Rev. Fluid Mech.*, 14, pp. 61-85.

Yates, L.A. and Chapman, G.T., 1992, "Streamlines, Vorticity Lines, and Vortices Around Three-Dimensional Bodies," *AIAA Journal*, Vol. 30, pp.1819-1826, June.

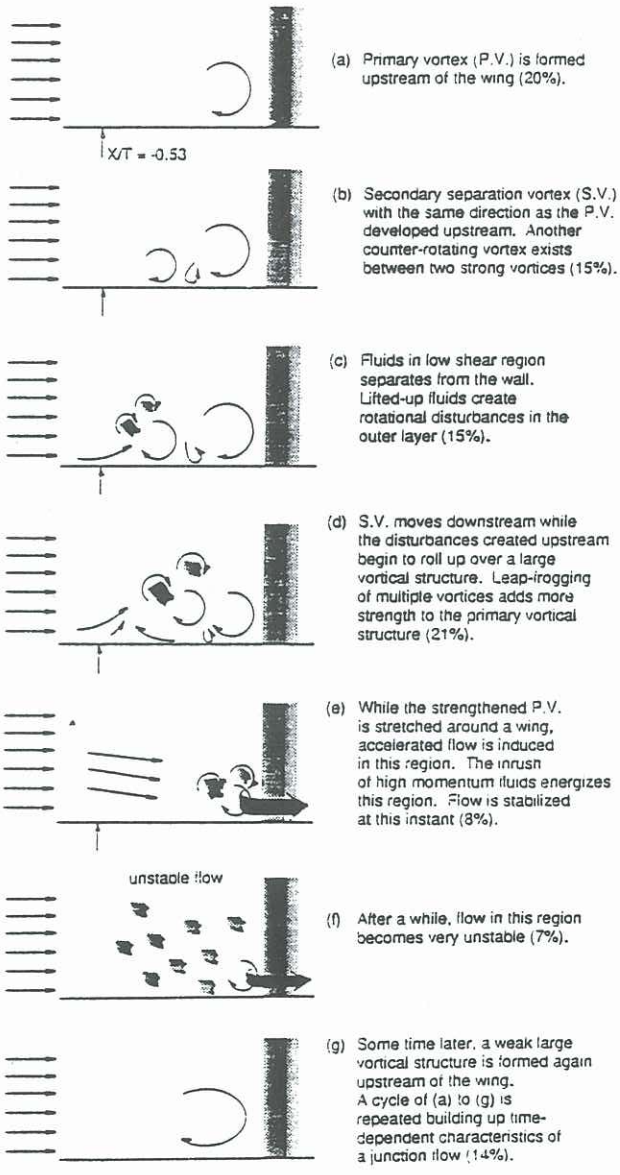

Figure 2. Descriptive model for the sequence of flow events in the nose region of a wing-body junction. The percentage in the parenthesis represents the approximate time proportion of the event. From Kim et al. (1991).